Inorganic Chemistry

Article

pubs.acs.org/IC

Enhanced High-Temperature Thermoelectric Performance of $Yb_{14-x}Ca_xMnSb_{11}$

Catherine A. Uvarov, Francisco Ortega-Alvarez, and Susan M. Kauzlarich*

Department of Chemistry, University of California, One Shields Avenue, Davis, California 95616, United States

Supporting Information

ABSTRACT: The high temperature *p*-type thermoelectric material $Yb_{14}MnSb_{11}$ has been of increasing research interest since its high temperature thermoelectric properties were first measured in 2006. Subsequent substitutions of Zn, Al, and La into the structure have shown that this material can be further optimized by altering the carrier concentration or by reduction of spin-disorder scattering. Here the properties of the $Yb_{14-x}Ca_xMnSb_{11}$ solid solution series where isovalent Ca^{2+} is substituted for Yb^{2+} will be presented. Crystals of the $Yb_{14-x}Ca_xMnSb_{11}$ solid solution series were made by Sn-flux (x = 2, 4, 6, 8) with the following ratio of elements: (14−x)Yb: xCa: 6 Mn: 11Sb: 86Sn, and their structures determined by single crystal X-ray diffraction. The density of the material significantly decreases by over 2 g/cm^3 as more Ca is added (from x = 1 to 8), because of the lighter mass of Ca. The resulting lower density is beneficial from a device manufacturing perspective where there is often a trade-off with the specific power per kilogram. The compounds crystallize in the $Ca_{14}AlSb_{11}$ structure type. The Ca substitution contributes to systematic lengthening the Mn−Sb bond while shortening the Sb−Sb bond in the 3 atom linear unit with increasing amounts of Ca. Temperature dependent thermoelectric properties, Seebeck, electrical resistivity, and thermal conductivity were measured from room temperature to 1273 K. Substitution of Yb with Ca improves the Seebeck coefficient while decreasing the thermal conductivity, along with decreasing the carrier concentration in this p-type material resulting in an enhanced thermoelectric figure of merit, zT, compared to $Yb_{14}MnSb_{11}$.

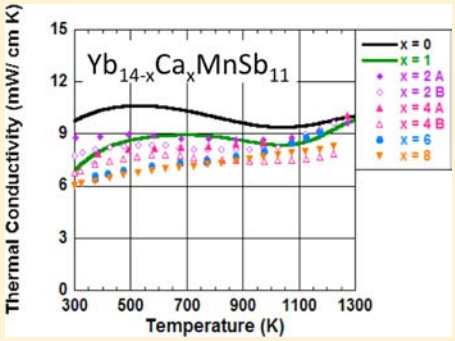

INTRODUCTION

Even though there are many Zintl phase structures known,[1] and many combinations of elements that comprise them, relatively few Zintl phases have been tested for their thermoelectric properties.[2] With the discovery of high thermoelectric figure of merit, zT, in $Yb_{14}MnSb_{11}$,[3] there has been significant interest in finding high zT in other Zintl phases.[4,5] Even for compounds with the same structure, finding the best combination of elements is crucial to have the optimal transport properties.[6] One Zintl phase that has been broadly studied has the general formula AM_2Sb_2 (A = Ca, Sr, Yb, Eu; M = Zn, Cd), of the structure type $CaAl_2Si_2$. Although all of the alkaline earth, rare earth, and transition metals are 2+ cations, the thermoelectric performance varies widely. For example, $Eu(Zn_{0.9}Cd_{0.1})_2Sb_2$ shows a maximum zT value of 1.06 at 650 K[7] while $CaCd_2Sb_2$ has a zT value close to 0 at the same temperature.[8] This was attributed to the transition from a heavily doped semiconductor to a metal. Isovalent substitution of elements into a system can subtly tune the transport properties to optimize the properties. In the case of AZn_2Sb_2 series, differences in the transport properties are attributed primarily to differences in mobility, and it has been suggested that these more ionic cations may provide an increase in point defects that lowers the lattice thermal conductivity.[9] $Yb_{14}MnSb_{11}$ is a Zintl phase of interest for high temperature thermoelectric applications since it has a zT = 0.8 at 1200 K.[3,10] So far, the only previous thermoelectric property study in the literature involving isovalent substitution in $Yb_{14}MnSb_{11}$ is for $Yb_{14}Mn_{1-x}Zn_xSb_{11}$[11] and $Yb_{13}CaMnSb_{11}$.[12] In this example, the increase in zT was attributed to reduction in electrical resistivity because of elimination of spin-mediated scattering. Preliminary investigation of Ca substitution, $Yb_{14-x}Ca_xMnSb_{11}$, suggested that this may be a promising direction for further studies.[12,13]

Several compounds are isostructural to $Yb_{14}MnSb_{11}$, generically described as $A_{14}MPn_{11}$ where A = alkaline earth or divalent rare earth, M = transition metal or group 13 element, and Pn = pnicogen and referred to as 14-1-11. The first compound reported with this structure type was $Ca_{14}AlSb_{11}$, and one formula unit consists of 14Ca^{2+} cations, 1 $[AlSb_4]^{9-}$ tetrahedron, 1 Sb_3^{7-} linear anion, and 4 Sb^{3-} anions. The crystal structure is shown in Figure 1.

Even though Ca^{2+} and Yb^{2+} in a 6 coordinate environment are essentially the same size (1.00 vs 1.01 Å), the unit cell for the $Ca_{14}MnSb_{11}$ is slightly larger. For $Ca_{14}MnSb_{11}$, room temperature (300 K) lattice parameters are a = 16.742(2) Å, c = 22.314(4) Å (V = 6254.5 Å^3),[14] and for $Yb_{14}MnSb_{11}$, the lattice parameters (300 K) are a = 16.617(1) Å, c = 21.999(1) Å (V = 6074.5 Å^3)[15]—equating to a 2.3% difference in volume. The origin for the expansion may be due in part to the difference in

Received: March 20, 2012
Published: July 3, 2012

 © 2012 American Chemical Society dx.doi.org/10.1021/ic300567c | *Inorg. Chem.* 2012, 51, 7617−7624

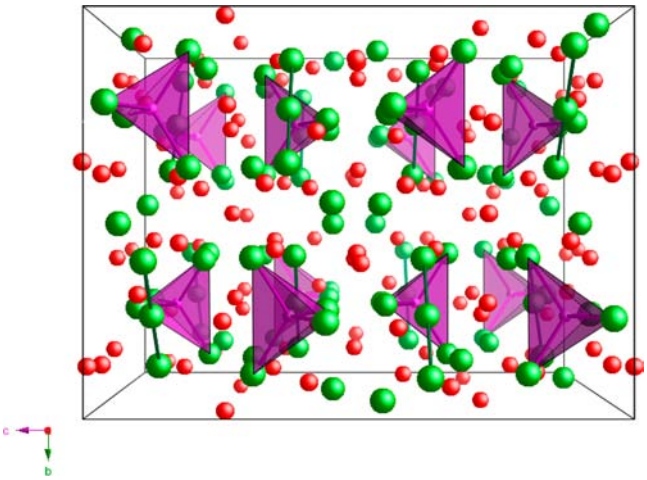

Figure 1. Crystal structure of $Yb_{14-x}Ca_xMnSb_{11}$. Shared Yb/Ca sites are shown in red, Mn in purple, and Sb are green.

bonding resulting from the difference in electronegativity of the two cations. Calcium is more electropositive than ytterbium thus making electron transfer more complete, resulting in more ionic bond character. The bond lengths between Ca−Sb in $Ca_{14}MnSb_{11}$ are longer than that in $Yb_{14}MnSb_{11}$, supporting this idea of more ionic character.[14,16] Theoretical calculations on $Ca_{14}GaAs_{11}$ and $A_{14}MnBi_{11}$ suggest that the alkaline earth ions in this structure type are ionic.[17,18] In the case of other Zintl phases, such as $YbZn_2Sb_2$ and $Yb_{11}GaSb_9$, the corresponding isostructural calcium analogues also have slightly larger unit cells suggesting that this observation is common across many Zintl phases.[19−22]

Creating the isovalent substitution of Yb with Ca, $Yb_{14-x}Ca_xMnSb_{11}$, across the entire x range should be possible because of the similarity of the elements and the fact that the two end members are isostructural.[13] The anticipated effect of calcium substitution on the thermoelectric properties is complex. First, the large mass difference between Ca and Yb will create significant mass/strain scattering that should lower lattice thermal conductivity.[4,13,23] Second, since Ca is more electropositive, the hole carrier concentration should decrease as observed in $Yb_{1-x}Ca_xZn_2Sb_2$.[23] The decrease in carrier concentration may be more pronounced because of the slightly increased unit cell volume. The carrier concentration in $Yb_{14}MnSb_{11}$ is too high, and previous results have shown that reducing the carrier concentration improves zT.[10,24,25] As an additional positive effect, substitution with the lighter Ca cation and larger cell volume results in dramatically reduced density. The density of $Ca_{14}MnSb_{11}$ is 4.091 g/cm^3 while $Yb_{14}MnSb_{11}$ is 8.368 g/cm^3.[14,16] Although this has little to do with the effect on thermoelectric properties, it is beneficial from a device manufacturing standpoint when zT specific power per gram of material is of concern.

Here the effect of Ca substitution is explored for samples prepared via Sn-flux synthesis, and their structure and high temperature thermoelectric properties of the hot pressed pellets were measured.

EXPERIMENTAL SECTION

Synthesis. All elements were handled using inert atmosphere techniques, including a nitrogen or argon filled glovebox with water levels <0.5 ppm. The elements Yb (Stanford Materials, 99.99%), and Ca (Alfa Aesar, 99.99%) were cut into small pieces. Sb metal (Baker Analyzed, 99.8%) and Mn pieces (Alfa Aesar, 99.95%) were ground into a course powder. Sn shot (Alfa Aesar, 99.98%) were used as received. The elements were layered into an Al_2O_3 crucible in the ratio (14−x)Yb: xCa: 6Mn: 11Sb: 86Sn with x = 2, 4, 6, 8. From this point on, all samples will be referred to by this synthetic x, designating the amount of Ca loaded into the reactions. The reaction was subsequently sealed in quartz under dynamic vacuum and heated up to 1000 °C according to the heating scheme previously described.[10] At 700 °C, the reactions were centrifuged at 6500 rpm for 3−5 min to remove the molten Sn from the crystals. The crystals were then harvested in a glovebox equipped with a microscope. Some single crystals were saved for further characterization while the majority of the sample was ball milled into a fine powder using a SPEX 8000 M in a 5 mL methacrylate vial with slip-on WC end-caps equipped with two 5/16″ WC balls for 5 min to grind the sample into a powder.

Table 1. Single Crystal XRD Refinement Parameters Where x = Reaction Stoichiometry for $Yb_{14-x}Ca_xMnSb_{11}$

parameter	x = 2	x = 4	x = 6	x = 8
experimental formula	$Yb_{11.802(6)}Ca_{2.198(6)}MnSb_{11}$	$Yb_{9.503(7)}Ca_{4.497(7)}MnSb_{11}$	$Yb_{8.050(7)}Ca_{5.950(7)}MnSb_{11}$	$Yb_{4.46(1)}Ca_{9.54(1)}MnSb_{11}$
crystal dimensions (mm)	0.33 × 0.16 × 0.11	0.14 × 0.08 × 0.08	0.43 × 0.17 × 0.10	0.14 × 0.08 × 0.05
space group	$I4_1/acd$	$I4_1/acd$	$I4_1/acd$	$I4_1/acd$
Z	8	8	8	8
temperature (K)	90(2)	90(2)	90(2)	90(2)
wavelength (Å)	0.71073	0.71073	0.71073	0.71073
lattice parameters (Å)	a = 16.5885(13)	a = 16.5853(13)	a = 16.5888(12)	a = 16.573(3)
	c = 21.9760(17)	c = 22.0353(18)	c = 22.0682(17)	c = 22.141(4)
volume (Å^3)	6047.3(8)	6061.3(8)	6072.9(8)	6081.3(19)
ρ_{calc} (g cm^{-3})	7.742	7.054	6.618	5.565
no. of collected reflections	35602	36332	36245	32422
no. of unique reflections	2209	2214	2221	1845
μ Mo Kα (mm^{-1})	46.468	39.744	35.498	25.132
2θ range (deg)	4.92 to 60	4.92 to 59.98	4.92 to 60	4.92 to 56
reflections collected	35602	36332	36245	32422
independent reflections	2209	2214	2221	1845
R1 [$I > 2\sigma(I)$][a]	0.0242	0.0344	0.0337	0.0590
wR2	0.0612	0.0684	0.0677	0.1394
largest diff. peak and hole (e Å^{-3})	2.159 and −2.390	3.696 and −3.544	3.289 and −2.980	3.038 and −3.152

[a] $R1 = \sum||F_o| - |F_c||/\sum|F_o|$; $wR2 = [\sum w(F_o^2 - F_c^2)^2]^{1/2}$; $w = [\sigma^2(F_o) + (0.0471P)^2 + (0.5945P)]$ where $P = [\max(F_o^2,0) + 2F_c^2/3]$.

dx.doi.org/10.1021/ic300567c | Inorg. Chem. 2012, 51, 7617−7624

Table 2. Selected Bond Lengths (Å) and Angles (deg) for Flux-Grown $Yb_{14-x}Ca_xMnSb_{11}$ Crystals Showing the Bonds with the Largest Changes Across the Series

	$x = 2$	$x = 4$	$x = 6$	$x = 8$
		Bond Length (Å)		
A(3)−Sb(1) × 2	3.3419(4)	3.3495(5)	3.3543(5)	3.3632(9)
A(4)−Sb(3)	3.1993(7)	3.2111(11)	3.2175(10)	3.229(3)
A(4)−Sb(3)	3.2146(7)	3.2219(10)	3.2251(10)	3.232(3)
A(4)−Sb(2) × 2	3.3945(7)	3.4017(10)	3.4074(10)	3.413(3)
Mn(1)−Sb(2) × 4	2.7492(5)	2.7546(7)	2.7581(7)	2.7620(14)
Sb(1)−Sb(4)	3.1826(7)	3.1785(10)	3.1764(10)	3.169(2)
		Bond Angle (deg)		
Sb(2)−Mn−Sb(2)	105.811(11)	106.098(15)	106.230(14)	106.61(3)
Sb(2)−Mn−Sb(2)″	117.07(2)	116.45(3)	116.17(3)	115.36(6)

Single Crystal X-ray Diffraction. In the drybox equipped with a microscope, small crystals were selected and transferred under paratone oil to the instrument. A suitable crystal was positioned onto a glass fiber and placed under a cold nitrogen stream (90 K) on a Bruker SMART 1000 CCD diffractometer utilizing a graphite-monochromatic Mo Kα radiation (λ = 0.71069 Å). Diffraction data were collected with the SMART software, and data reduction performed with SAINT version 6.45. A multiscan absorption correction was applied using SADABS. The initial atom positions were taken from a previously published $Yb_{14}MnSb_{11}$ structure,[16] and refined with SHELXTL version 5.1. Occupancies of the shared Yb and Ca sites were allowed to refine with the positional parameters restrained to be equivalent. Table 1 provides a summary of data collection and refinement parameters. Table 2 provides selected bond lengths and angles. The x = 8 sample had problems with the higher angle data, and the data set was truncated slightly compared with the others. The x = 8 crystal may have distinct domains of varying Ca content, as imaged in the microprobe.

Electron Microprobe Analysis. Randomly selected crystals from each composition were analyzed using a Cameca SX-100 Electron Probe Microanalyzer equipped with a wavelength-dispersive spectrometer with 20 keV accelerating potential and 10 nA beam current. The samples were mounted in epoxy and polished to a mirror-like finish. The epoxy and sample was carbon coated for better conduction. Net elemental intensities for Yb, Mn, and Sb were determined with respect to pure elemental polished calibration standards, and $CaMoO_4$ was used for net elemental intensities of Ca. The composition of each sample was determined by calculating averages and standard deviations from 15 to 30 randomly selected data points of the main phase.

Powder X-ray Diffraction. X-ray diffraction (XRD) data were collected on powder of each sample using a Bruker airtight holder. Room temperature XRD data were collected at room temperature on a Bruker D8 Advance Diffractometer operated at 40 kV and 40 mA utilizing Cu Kα_1 radiation. MDI JADE 6.1 software was used for background subtraction and pattern analysis. Whole pattern fitting (WPF) was performed using MDI JADE 6.1 software against calculated patterns from the single crystal XRD refinements, and Sn from the ICSD database.[26]

Consolidation of Powder. The powder of ground crystals was consolidated into a dense pellet via hot-pressing in high-density graphite dies (POCO) at about 20,000 psi and 1223 K for 1.5 h under argon, leading to sample density >95% of the theoretical density by the Archimedes method.

Thermoelectric Properties. The van der Pauw technique was used to measure the electrical resistivity (ρ) with a current of 100 mA and a special high-temperature apparatus.[27] The Hall coefficient was measured simultaneously on the same instrument utilizing a forward and reverse magnetic field value of about 8000 G. The carrier density (n) was calculated from the Hall coefficient (R_H) assuming a scattering factor of 1.0 in a single-carrier scheme, with $n = 1/R_He$, where n is the charge carrier density and e the charge of the electron. The Hall mobility (μ_H) was calculated from the Hall coefficient and resistivity values with $\mu_H = R_H/\rho$. The thermal diffusivity was measured using a flash diffusivity technique.[28] The heat capacity was calculated using the experimental heat capacity for $Yb_{14}MnSb_{11}$,[10] correcting for the molar mass of Ca based on the compositions determined from microprobe analysis. The thermal conductivity (κ) was derived from the heat capacity,[10] experimental density, and experimental thermal diffusivity values. The Seebeck coefficient (S) was measured using a high-temperature light pulse technique using W/Nb thermocouples.[29] All data were collected to 1273 K, and fit with high order polynomial functions using Origin 8 and extrapolated to 1300 K for zT calculations. Thermoelectric properties for x = 0 ($Yb_{14}MnSb_{11}$)[3] and x = 1,[13] were taken from previously published results, with the heat capacity correction mentioned above.

RESULTS AND DISCUSSION

Single Crystal XRD. Preparation of single crystals of $Yb_{14}MnSb_{11}$ using molten Sn as a solvent (flux) with a typical ratio of elements as 14Yb: 6 Mn: 11Sb: 86Sn has been reported by this research group.[3,10,11,13,15,24,30−34] Flux growth techniques have some advantages over traditional solid state methods including: (1) crystals of materials can be synthesized below their melting points, (2) impurities are often minimized or removed by the flux, and (3) chemical substituted variants can be made easily. Simply by replacing some Yb with Ca, in the flux, we were able to prepare single crystals of the solid solution series, $Yb_{14-x}Ca_xMnSb_{11}$ ($0 < x \leq 8$).

A high yield of metallic-gray crystals, ranging in size from less than 1 mm to several mm across, was obtained from each Sn-flux reaction. A crystal chosen at random from each composition (x = 2, 4, 6, 8) was selected for full data collection and structural refinement. The data collection and refinement parameters are summarized in Table 1. The structure of each composition refined in the $I4_1/acd$ space group with lattice parameters similar to previous 14-1-11 compounds.

Table 1 shows that there is no significant change in lattice parameter a, whereas c increases with increasing Ca content by 0.165(4) Å going from x = 2 to 8. Increasing lattice parameters were also observed with Al doping, where c increased by approximately 0.17 Å going from Al = 0.2 to 0.95 and a remained essentially constant.[10] In general, the structurally refined value of x is larger than the synthetic x (the amount used in the flux reaction), for example for x = 4 the refined x was 4.497(7). This is only possible if there is a decrease in the overall yield or if there is more Ca in some crystals than in others. Because of the lighter mass of Ca while slightly increasing the volume of the unit cell, the density of the material significantly drops as more Ca is added by over 2 g/cm^3 going from x = 2 to 8. This is beneficial from a device perspective where there is often a trade-off between the weight of the device and its efficiency. If the zT is maintained, the

dx.doi.org/10.1021/ic300567c | Inorg. Chem. 2012, 51, 7617−7624

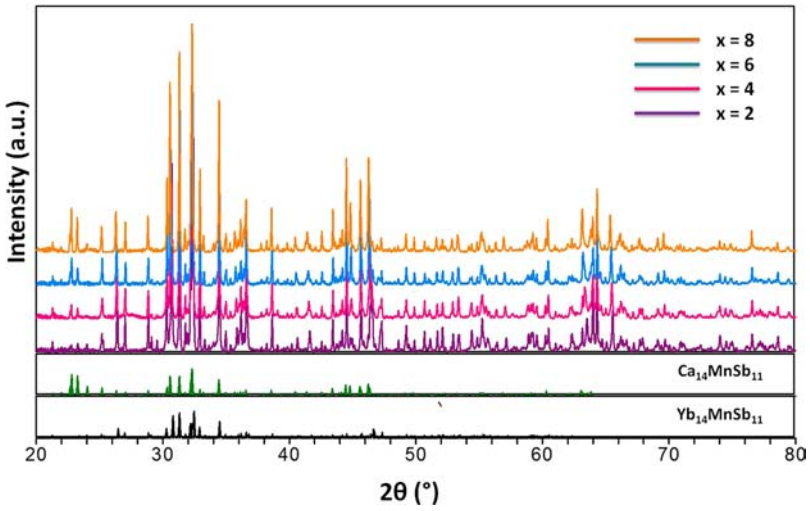

Figure 2. Powder XRD patterns for flux grown $Yb_{14-x}Ca_xMnSb_{11}$. Calculated patterns for $Ca_{14}MnSb_{11}$ and $Yb_{14}MnSb_{11}$ are shown for reference.

Table 3. Summary of Whole Pattern Fitting of Powder XRD Data for Flux Grown Compositions

x	a (Å)	c (Å)	wt % $Yb_{14-x}Ca_xMnSb_{11}$	wt % Sn	R (%)
x = 2	16.6216(7)	22.028(1)	97(2)	3.3(3)	3.81
x = 4	16.6233(6)	22.1123(9)	97(2)	3.0(3)	4.09
x = 6	16.6217(7)	22.159(1)	97(2)	2.8(3)	3.92
x = 8	16.6295(6)	22.205(1)	96(2)	4.4(5)	3.82

output per gram of material can be increased by the addition of calcium.

The bond distances show changes <1% going across the series, with the largest changes between the shared Yb/Ca sites (A) and neighboring Sb atoms, as shown in Table 2. There is also a minor increase in Mn−Sb bonds in the tetrahedral and a decrease in Sb−Sb bonds in the linear chain by approximately 0.5%. The bond angles of the tetrahedron become closer to ideal (109.5°) as more Ca is added (Table 2). The top of the Fermi level should be a mixture of the $[MnSb_4]^{9-}$ tetrahedron and the Sb_3^{7-} linear unit bonding orbitals.[17] Therefore, it is expected that the additional electronic density from replacing Yb^{2+} with Ca^{2+} should affect those bonds the most. Adding additional electron density may elongate the Mn−Sb bond since the additional electron density fills the hole and reduces the interaction between the Mn and Sb in the tetrahedron and shorten the Sb_3^{7-} linear anion as it contributes to bonding. The slight increase in A-Sb bond lengths along with the removal of the distortion of the tetrahedron with increasing Ca content may be the main contributors to the lattice parameter increase in the c direction, as both would influence the packing in the structure. Additionally, slight changes in the filling of the states at the Fermi level (as indicated by reduction of carrier concentration, see discussion below) may also play a role. The role of the Sb_3^{7-} unit has been examined with respect to its electronic contribution to the density of states (DOS).[35] Similar to what has been observed in other theoretical calculations,[17,18] while the orbitals are at the top of the Fermi level, they are localized and the bonding is in good agreement with the idea of a hypervalent species with a bond order of 1/2. The observation that they become shorter may be due to either matrix effects (the cation substitution and resulting size of the unit cell) or filling of the hole that is associated with the $MnSb_4^{9-}$ tetrahedron.[17]

The ionic radii of Ca^{2+} and Yb^{2+} in 6 coordinate environments are virtually identical (1.00 vs 1.02 Å).[36] The coordination environment of the crystallographic sites is roughly octahedral; however, the site for A(2), where A = Ca, Yb in this example, is significantly distorted. The symmetry of the different cation sites has been described in detail before for 14-1-11 compounds.[37] The percentage of Ca at each crystallographic site is roughly constant across the series with 31% at A(2), 31% at A(4), 24% at A(1), and 14% at A(3). This order of occupation preferences is reverse from that found for Ca substitution in $Eu_{14}MnSb_{11}$.[38,39] In the case of $Eu_{13}CaMnSb_{11}$, Ca preferentially occupied A(3) the most, then A(1), A(4), and last A(2).[37] However, it is important to note that size may play a role; Ca^{2+} is smaller than Eu^{2+} (1.17 Å), whereas it is similar size to Yb^{2+}.[36] For $Eu_{13}AMnSb_{11}$, when A is larger than Eu (such as Sr^{2+} and Ba^{2+}) the trend is the same as reported in this case.[37] The larger cation needs more space and preferentially occupies the most distorted site first. In this case, the occupation of the sites suggests Ca^{2+} is larger than Yb^{2+}, despite similar literature radii where Yb^{2+} is slightly larger. The more ionic nature of Ca^{2+} may be reflected in the effect of Ca^{2+} acting as a larger cation compared to Yb^{2+}, and this correlates well to the observed slight increase in bond lengths with neighboring Sb. Additionally, since Ca is more electropositive, it can donate slightly more electron density to Sb making the bond more ionic in character.

The slight reduction in the angle in the $MnSb_4^{9-}$ species and the Sb_3^{7-} bond may be due to matrix effects as mentioned above. It is also possible since there is a reduction in the carrier concentration that this is due to defects whose numbers are too small to be detected[40] or that the slight increase in electron donation affects the structure of $MnSb_4^{9-}$, diminishing the effect of the polarized hole and thereby making the angle more ideal, that is, more toward 109°. Since the additional electron density is not expected to contribute to bonding or antibonding

dx.doi.org/10.1021/ic300567c | Inorg. Chem. 2012, 51, 7617−7624

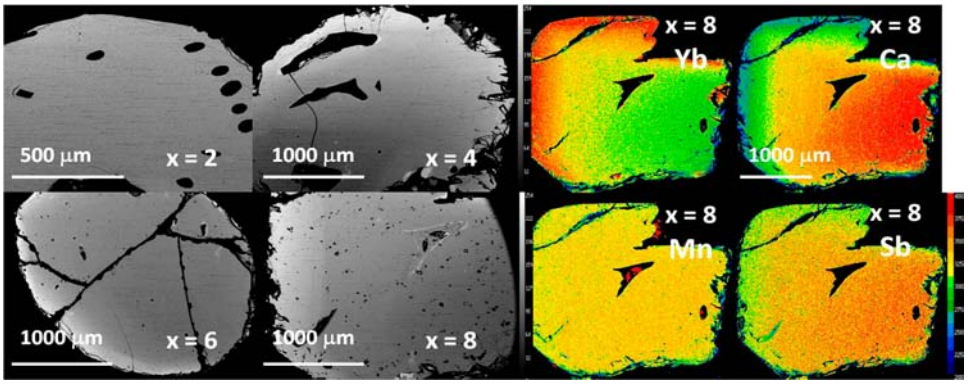

Figure 3. Backscattered electron images for single crystals made by Sn-flux on left, and elemental maps for the $x = 8$ crystal on the right. The black areas within the crystal are Sn inclusions.

orbitals of the Sb_3^{7-} trimer, the observed slight shortening with increasing Ca^{2+} is likely a synergistic effect associated with the cation substitution and tetrahedron angle change rather than a direct electronic effect.

Powder XRD. Crystals from flux-grown $Yb_{14-x}Ca_xMnSb_{11}$ were ground into a fine powder by ball milling for 5 min. The powder XRD patterns, Figure 2, are consistent for pure 14-1-11 phase materials with residual Sn from the synthetic route.

The gradual change from predominantly Yb ($x = 2$) to Ca ($x = 8$) is most clearly observed at low angle (22−28° 2θ) with the increase in intensity with Ca. With close inspection, slight change in peak positions is also observed. Whole pattern fitting using Jade 6.1 software reveals lattice parameter trends similar to that observed in single crystal XRD refinements, Table 3, where a remains essentially constant and c gradually increases with increasing Ca content. Throughout the series, the amount of residual flux is approximately 3%, but varies for each synthesis batch depending on how much was removed during centrifugation.

Electron Microprobe Analysis. From backscattered electron (BSE) images for flux-grown crystals, a gradation was observed across the polished surface, shown on the left in Figure 3. To better show this subtle change in composition, elemental maps of the entire crystal surface are shown on the right in Figure 3 for the $x = 8$ crystal. The crystals appear to be higher in Ca concentration on one side, or toward the center, and then become more Yb rich toward the outer rim. Also interesting to note is that the distribution of Mn is homogeneous, but Sb is not. The inhomogeniety of Sb is somewhat surprising, but the variation in concentration is less drastic than that of Ca or Yb. The Sb appears slightly higher in concentration where the crystal is Ca rich. This is not the first time that a slight amount of extra Sb appears in Ca-containing 14-1-11 compounds. For $Ca_{14}ZnSb_{11}$ and $Ca_{14}CdSb_{11}$, microprobe analysis also suggested higher Sb concentrations, and an interstitial Sb was modeled into the single crystal XRD data because of residual electron density near Sb(3).[41] There was no significant amount of residual electron density that might prompt the use of a similar model for the single crystal refinements discussed previously in this paper. The composition for each crystal, calculated from several WDS data points, is reported in Table 4. The composition for each crystal varies depending on where on the crystal the data was taken, and it probably varies from crystal to crystal within a batch. As such, the determined composition from single crystal XRD differs from that determined by microprobe.

Table 4. Composition Determined from Electron Microprobe Analysis

	composition
$x = 1$	$Yb_{12.8(3)}Ca_{1.2(1)}Mn_{0.96(4)}Sb_{11.0(3)}$
$x = 2$	$Yb_{12.78(5)}Ca_{0.69(7)}Mn_{0.977(4)}Sb_{11.00(4)}$
$x = 4$	$Yb_{9.3(6)}Ca_{4.2(6)}Mn_{0.982(4)}Sb_{11.00(2)}$
$x = 6$	$Yb_{6.1(7)}Ca_{7.5(7)}Mn_{0.979(5)}Sb_{11.00(3)}$
$x = 8$	$Yb_{4.9(6)}Ca_{8.6(6)}Mn_{0.975(6)}Sb_{11.00(2)}$

Thermoelectric Properties. As the amount of Ca increases in these samples, the air-sensitivity also increases making the samples more difficult to handle without damaging oxidation. Consolidation of the powder into a dense pellet was also difficult for the higher x compounds. Separate batches of each stoichiometry were hot-pressed; however, only one pellet for $x = 6$ and $x = 8$ were successfully densified. The thermal conductivity on all samples is shown below in Figure 4. Only the thermal conductivity data on $x = 6$ and $x = 8$ was collected because of the high level of sample oxidation.

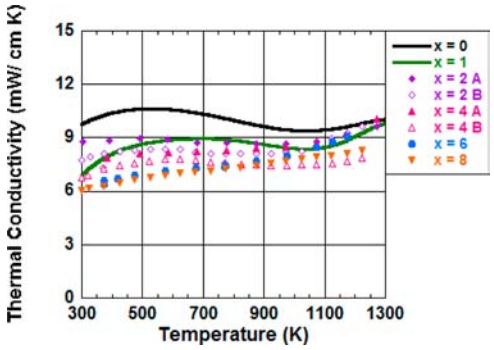

Figure 4. Thermal conductivity decreases when Ca is substituted for Yb because of mass/strain scattering. Thermal conductivity data shown for all $Yb_{14-x}Ca_xMnSb_{11}$ samples made by Sn-flux ($x = 2$ and 4 were measured for two different pellets).

To apply the heat capacity correction to the thermal conductivity, the molar mass of the compound needs to be calculated, and the molar mass is heavily dependent on the amount of Ca in each composition. For Figure 4, the molar mass was calculated assuming the Ca content determined by electron microprobe analysis on single crystals, reported in Table 4. The thermal conductivity for $x = 0$, $Yb_{14}MnSb_{11}$, from Brown et al.[3] was corrected for heat capacity also. Although it

dx.doi.org/10.1021/ic300567c | Inorg. Chem. 2012, 51, 7617−7624

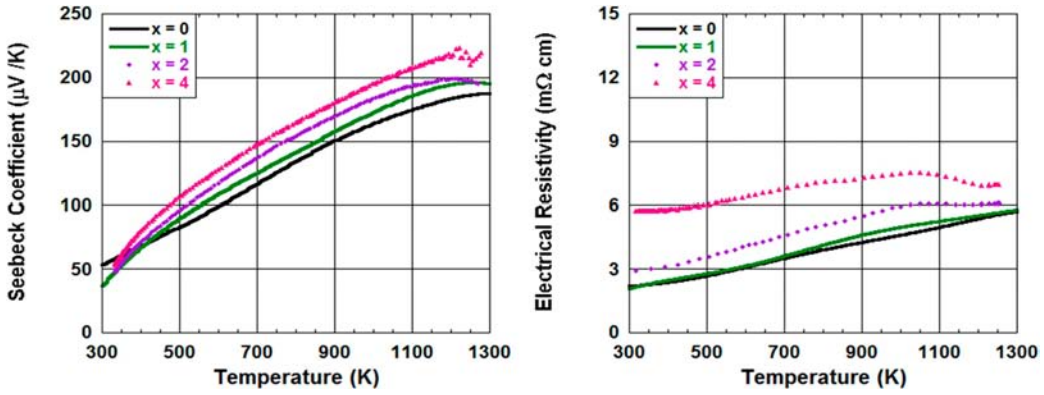

Figure 5. Seebeck coefficient and electrical resistivity as a function of temperature for Sn-flux made $Yb_{14-x}Ca_xMnSb_{11}$ samples for $x = 0-4$.

may not be ideal, the application of the $Yb_{14}MnSb_{11}$ experimental heat capacity to this solid solution series provides a conservative estimate of the thermal conductivity. Whatever constant used would show the same trend, but the Dulong-Petit estimate gives notably lower thermal conductivity (which would give inflated zT), so the experimental heat capacity was applied. There is a reduction in the thermal conductivity for the Ca containing samples, as expected, because of the large mass difference between Yb and Ca. The reduction in thermal conductivity is fairly systematic at low temperatures, with $x = 6$ and $x = 8$ having the lowest thermal conductivity (6.03 mW/cm K for $x = 8$ at room temperature). As the temperature increases, the systematic ordering of the thermal conductivities diminishes. The thermal conductivity also varies slightly from batch to batch, perhaps depending on how much Ca was incorporated during the synthesis.

The reduction in thermal conductivity as Ca is added is similar to that observed when Al was added. In that case, Al = 0.95 had the lowest room temperature thermal conductivity, 5.90 mW/cm K.[10] In the Al series, Al = 0.6 and Al = 0.8 had the maximum zT of 1.1 at 1223 K.[10,24] The high temperature (1200 K) thermal conductivity values for Al = 0.6 and Al = 0.8 were near 6.0−7.5 mW/cm K.[10,24] The samples corresponding to $x =$ 2A and $x =$ 4A were the only samples intact after thermal conductivity measurements to obtain Seebeck coefficient and electrical resistivity data. The thermal conductivity at 1200 K values for $x =$ 2A and 4A were, respectively, 9.16 and 9.18 mW/cm K, higher than that for the ideal Al-substituted compounds.

The carrier concentration of $Yb_{14}MnSb_{11}$ is about 1.35×10^{21} holes/cm^3 corresponding to about one hole per Mn (1.3×10^{21} holes/cm^3).[34] The carrier concentrations for $x = 2$ and $x =$ 4 were found to be about $8.3(8) \times 10^{20}$ and $3.3(2) \times 10^{20}$ holes/cm^3, respectively, at room temperature (300 K). This is similar to the optimum range of carrier concentration found for Al^{3+} substitution ($Yb_{14}Mn_{1-x}Al_xSb_{11}$), where Al = 0.6 and Al = 0.8 had carrier concentrations of about 7×10^{20} and 4×10^{20} holes/cm^3, respectively.[10,24] Even though Ca is isovalent with Yb, this substitution has a profound effect on n, as demonstrated by the Al-substituted n values being between the n values for $x = 2$ and $x = 4$. This may be explained by the more ionic bonding character of Ca^{2+} compared to Yb^{2+}. Using simple electron-donation ideas, Ca is more electropositive and will therefore donate more electron density to the system, lowering the number of holes. As discussed previously, A-Sb bond lengths elongate as Ca is added supporting the idea that electron transfer is more complete with Ca than Yb. The decrease in the carrier concentration with increasing Ca content is reflected in the high temperature Seebeck coefficient and electrical resistivity measurements (Figure 5).

As the carrier concentration decreases, the Seebeck coefficient and electrical resistivity rise since both properties are inversely related to the carrier concentration. The maximum Seebeck coefficient reached by $x = 4$ is 217 μV/K at 1250 K and 198 μV/K at 1200 K for $x = 2$. This is a bit lower than the maximum Seebeck coefficient reached for the Al = 0.6 and Al = 0.8, despite having similar carrier concentration. In that case, the Al = 0.8 sample had a maximum Seebeck coefficient of 255 μV/K at 1125 K.

$$\alpha = \frac{8\pi^2 k_B^2}{3eh^2} m \times T\left(\frac{\pi}{3n}\right)^{2/3} \quad (1)$$

The effective mass can be estimated from the slope of the lower temperature Seebeck data (dS/dT) at $T \approx 500-700$ K and the carrier concentrations listed above using the eq 1 provided above. The effective mass is ~2.7 m_e for $x = 2$ and ~1.4 m_e for $x = 4$. The value of 2.7 m_e is close to the Al series where the effective mass was close to 3 m_e for the entire series.

The electrical resistivity of $x = 2$ attains a plateau at 1000 K at 6 mΩ cm. The $x = 4$ sample reaches a maximum of 7.5 mΩ cm at 1025 K and decreases to 6.9 mΩ cm at 1200 K. When compared to the Al-substituted compounds, the $x = 2$ and $x = 4$ Ca substituted samples have lower electrical resistivity than Al = 0.6 and 0.8, Al = 0.6 having electrical resistivity at 1200 K of 8.4 mΩ cm. Overall, the Ca substitution ($x = 2$ and 4) provides higher thermal conductivity, lower Seebeck coefficient, and lower electrical resistivity when compared to the optimal Al-substituted compounds. Substitution with Ca improves the zT compared to $Yb_{14}MnSb_{11}$ (Figure 6). The Ca substitution changes the properties in a systematic fashion, with the Seebeck coefficient slowly increasing, along with electrical resistivity. The thermal conductivity initially is reduced, but additional reduction with increasing amounts of Ca is not significant. Therefore, we see improvement initially, but as the electrical resistivity becomes high for the $x = 4$, we see the zT decrease. When zT is calculated, the highest zT is obtained with the $x = 1$ sample. Presumably, the reduction of the carrier concentration to the optimal range happens at or below $x = 4$. This is good because higher Ca concentrations are too air sensitive to work with easily.

■ CONCLUSION

$Yb_{14-x}Ca_xMnSb_{11}$ is a complex structure that has been made in high-yield by growing crystals in a Sn-flux. Subtle but systematic

dx.doi.org/10.1021/ic300567c | Inorg. Chem. 2012, 51, 7617−7624

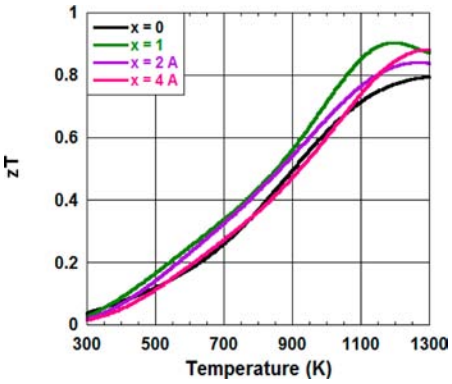

Figure 6. Thermoelectric figure of merit, zT, as a function of temperature for x = 1, 2, and 4.

changes in structure occur with increasing Ca composition. Compositions with high values of x were too air-sensitive to withstand thermoelectric property measurements to high temperatures. The substitution of Ca for Yb reduces the carrier concentration resulting in increased Seebeck coefficient and electrical resistivity. The large mass difference between Ca and Yb also produces mass-disorder scattering, lowering the lattice thermal conductivity. The overall effect is increased zT over $Yb_{14}MnSb_{11}$; however, the improvement was not as dramatic as observed via Al substitution. Since Ca substitution reduces the density, some Ca-substitution may be useful for device fabrication. The $Yb_{14-x}Ca_xMnSb_{11}$ solid solution may be further enhanced with additional elemental substitutions.

■ ASSOCIATED CONTENT

Supporting Information

X-ray crystallographic files in CIF format. This material is available free of charge via the Internet at http://pubs.acs.org.

■ AUTHOR INFORMATION

Corresponding Author

*E-mail: smkauzlarich@ucdavis.edu.

Notes

The authors declare no competing financial interest.

■ ACKNOWLEDGMENTS

This research was funded by NSF, DMR-0600742. The authors gratefully acknowledge Dr. Sarah Roeske and Brian Joy for the microprobe analysis and the Jet Propulsion Laboratory (JPL) for the thermoelectric measurements. We would also like to thank Eric Toberer and G. Jeffrey Snyder of the California Institute of Technology and Sabah Bux and Jean-Pierre Fleurial (JPL) for their assistance with the measurements.

■ REFERENCES

(1) Kauzlarich, S. M. *Chemistry, Structure, and Bonding of Zintl Phases and Ions*; VCH Publishers, Inc: New York, 1996.
(2) Kauzlarich, S. M.; Brown, S. R.; Snyder, G. J. *Dalton Trans.* **2007**, No. 21, 2099–2107.
(3) Brown, S. R.; Kauzlarich, S. M.; Gascoin, F.; Snyder, G. J. *Chem. Mater.* **2006**, *18* (7), 1873–1877.
(4) Toberer, E. S.; May, A. F.; Snyder, G. J. *Chem. Mater.* **2010**, *22* (3), 624–634.
(5) Toberer, E. S.; Zevalkink, A.; Crisosto, N.; Snyder, G. J. *Adv. Funct. Mater.* **2010**, *20*, 4375–4380.
(6) Zevalkink, A.; Toberer, E. S.; Bleith, T.; Flage-Larsen, E.; Snyder, G. J. *J. Appl. Phys.* **2011**, *110* (1), 013721.
(7) Zhang, H.; Baitinger, M.; Tang, M. B.; Man, Z. Y.; Chen, H. H.; Yang, X. X.; Liu, Y.; Chen, L.; Grin, Y.; Zhao, J. T. *Dalton Trans.* **2010**, *39* (4), 1101–1104.
(8) Cao, Q. G.; Zhang, H.; Tang, M. B.; Chen, H. H.; Yang, X. X.; Grin, Y.; Zhao, J. T. *J. Appl. Phys.* **2010**, *107* (5), 053714.
(9) Toberer, E. S.; May, A. F.; Melot, B. C.; Flage-Larsend, E.; Snyder, G. J. *Dalton Trans.* **2010**, *39*, 1046–1054.
(10) Cox, C. A.; Toberer, E. S.; Levchenko, A. A.; Brown, S. R.; Snyder, G. J.; Navrotsky, A.; Kauzlarich, S. M. *Chem. Mater.* **2009**, *21* (7), 1354–1360.
(11) Brown, S. R.; Toberer, E. S.; Ikeda, T.; Cox, C. A.; Gascoin, F.; Kauzlarich, S. M.; Snyder, G. J. *Chem. Mater.* **2008**, *20* (10), 3412–3419.
(12) Uvarov, C. A.; Rauscher, J. F.; Kauzarich, S. M. *Sci. Adv. Mater.* **2011**, *3*, 646–651.
(13) Cox, C.; Brown, S.; Snyder, G.; Kauzlarich, S. *J. Electron. Mater.* **2010**, *39* (9), 1373–1375.
(14) Rehr, A.; Kuromoto, T. Y.; Kauzlarich, S. M.; Delcastillo, J.; Webb, D. J. *Chem. Mater.* **1994**, *6* (1), 93–99.
(15) Rauscher, J. F.; Cox, C. A.; Yi, T. H.; Beavers, C. M.; Klavins, P.; Toberer, E. S.; Snyder, G. J.; Kauzlarich, S. M. *Dalton Trans.* **2010**, *39* (4), 1055–1062.
(16) Chan, J. Y.; Olmstead, M. M.; Kauzlarich, S. M.; Webb, D. J. *Chem. Mater.* **1998**, *10* (11), 3583–3588.
(17) Sánchez-Portal, D.; Martin, R. M.; Kauzlarich, S. M.; Pickett, W. E. *Phys. Rev. B: Condens. Matter Mater. Phys.* **2002**, *65* (14), 144414.
(18) Gallup, R. F.; Fong, C. Y.; Kauzlarich, S. M. *Inorg. Chem.* **1992**, *31*, 115–118.
(19) Mewis, A. *Z. Naturforsch., B: Chem. Sci.* **1978**, *33* (4), 382–384.
(20) Pfleiderer, C.; Vollmer, R.; Uhlarz, M.; Faisst, A.; Von Lohneysen, H.; Nateprov, A. *Phys. B: (Amsterdam, Neth.)* **2002**, *312*, 352–353.
(21) Bobev, S.; Fritsch, V.; Thompson, J. D.; Sarrao, J. L.; Eck, B.; Dronskowski, R.; Kauzlarich, S. M. *J. Solid State Chem.* **2005**, *178* (4), 1071–1079.
(22) Young, D. M.; Kauzlarich, S. M. *Chem. Mater.* **1995**, *7* (1), 206–209.
(23) Gascoin, F.; Ottensmann, S.; Stark, D.; Haile, S. M.; Snyder, G. J. *Adv. Funct. Mater.* **2005**, *15* (11), 1860–1864.
(24) Toberer, E. S.; Cox, C. A.; Brown, S. R.; Ikeda, T.; May, A. F.; Kauzlarich, S. M.; Snyder, G. J. *Adv. Funct. Mater.* **2008**, *18* (18), 2795–2800.
(25) Toberer, E. S.; Brown, S. R.; Ikeda, T.; Kauzlarich, S. M.; Snyder, G. J. *Appl. Phys. Lett.* **2008**, *93* (6), 062110.
(26) *Inorganic Crystal Structure Database*; National Institute of Standards and Technology: Gaithersburg, MD, 2004; Vol. *1.3.3*.
(27) McCormack, J. A.; Fleurial, J. P. *Mater. Res. Soc. Symp. Proc.* **1991**, *234*, 135–143 (Mod. Perspect. Thermoelectr. Relat. Mater.).
(28) Vandersande, J. W.; Wood, C.; Zoltan, A.; Whittenberger, D. *Therm. Cond.* **1988**, *19*, 445–452.
(29) Wood, C.; Zoltan, D.; Stapfer, G. *Rev. Sci. Instrum.* **1985**, *56* (5), 719–722.
(30) Fisher, I. R.; Wiener, T. A.; Bud'ko, S. L.; Canfield, P. C.; Chan, J. Y.; Kauzlarich, S. M. *Phys. Rev. B: Condens. Matter Mater. Phys.* **1999**, *59* (21), 13829–13834.
(31) Burch, K. S.; Schafgans, A.; Butch, N. P.; Sayles, T. A.; Maple, M. B.; Sales, B. C.; Mandrus, D.; Basov, D. N. *Phys. Rev. Lett.* **2005**, *95* (4), 046401.
(32) Holm, A. P.; Kauzlarich, S. M.; Morton, S. A.; Waddill, G. D.; Pickett, W. E.; Tobin, J. G. *J. Am. Chem. Soc.* **2002**, *124* (33), 9894–9898.
(33) Ribeiro, R. A.; Hadano, Y.; Narazu, S.; Suekuni, K.; Avila, M. A.; Takabatake, T. *J. Phys.: Condens. Matter* **2007**, *19*, 376211.
(34) Sales, B. C.; Khalifah, P.; Enck, T. P.; Nagler, E. J.; Sykora, R. E.; Jin, R.; Mandrus, D. *Phys. Rev. B: Condens. Matter Mater. Phys.* **2005**, *72* (20), 205207.
(35) Xu, J.; Kleinke, H. *J. Comput. Chem.* **2008**, 2134–2143.

(36) Giacovazzo, C.; Monaco, H. L.; Viterbo, D.; Scordari, F.; Gilli, G.; Zanotti, G.; Catti, M. *Fundamentals of Crystallography*; IUCr-Oxford University Press: New York, 1992; p 654.
(37) Kim, H.; Klavins, P.; Kauzlarich, S. M. *Chem. Mater.* **2002**, *14* (5), 2308−2316.
(38) Kim, H.; Chan, J. Y.; Olmstead, M. M.; Klavins, P.; Webb, D. J.; Kauzlarich, S. M. *Chem. Mater.* **2002**, *14*, 206−216.
(39) Kim, H.; Olmstead, M. M.; Klavins, P.; Webb, D. J.; Kauzlarich, S. M. *Chem. Mater.* **2001**, *14*, 3382−3390.
(40) May, A. F.; McGuire, M. A.; Ma, J.; Delaire, O.; Huq, A.; Custelcean, R. *J. Appl. Phys.* **2012**, *111*, 033708.
(41) Young, D. M.; Torardi, C. C.; Olmstead, M. M.; Kauzlarich, S. M. *Chem. Mater.* **1995**, *7* (1), 93−101.